



SEISMIC DAMAGE BEHAVIOUR OF AEOLIAN SAND REINFORCED CONCRETE COLUMNS WITH I-SHAPED STRUCTURAL STEEL

Y. H. WANG^{1,2}, H. Y. WANG², Y. P. WANG², M. ZHAO², J. QI², G. Z. HUO²,
P. Q. LIU²

To promote the application of aeolian sand resources for steel-concrete composite structures, an aeolian sand reinforced concrete column with I-shaped structural steel is proposed in this study. Four specimens are designed and manufactured with different replacement rates of aeolian sand. The seismic behaviour and damage evolution process of the specimens are studied by low-cycle repeated loading tests. Based on the test results, the mechanical characteristics, failure modes, hysteresis curves, skeleton curves, energy dissipation capacity, displacement ductility, and stiffness degradation of the specimens with different replacement rates of aeolian sand are analysed. In addition, the effects of the design parameters on the seismic behaviour of the specimens are also studied. The results show that the indexes of the seismic behaviour can be significantly improved by adding steel. Moreover, a revised damage model is proposed, to better reflect the evolution law of seismic damage of aeolian sand reinforced concrete columns with steel. The proposed model can provide an important reference for seismic damage assessment of the columns.

Keywords: aeolian sand; columns; I-shaped structural steel; seismic damage behaviour; damage model

¹ Associate Prof., PhD., Inner Mongolia University of Technology, Inner Mongolia Key Laboratory of Civil Engineering Structures and Mechanics, Hohhot, China, e-mail: wyh@imut.edu.cn

² School of Civil Engineering, Inner Mongolia University of Technology, Hohhot, China, e-mail: 20181800271@imut.edu.cn

1. INTRODUCTION

Due to the global desertification, the living environment is also deteriorating. With the continuous increase in the construction of various domestic infrastructures and rapid urbanization, the demand for river sands is increasing. As a result, the natural sand resources with highly uneven natural distributions have been increasingly exhausted. In this context, aeolian sand can be mixed with concrete to reduce the dependence on natural sand and alleviate the damage to aeolian sand, which shows far-reaching significance for environmental protection. In recent years, many studies have been conducted on aeolian sand concrete.

Many scholars at home and abroad have done a lot of research on the seismic behaviour of reinforced concrete structures[1-7]. W. Dong et al. [8] mixed the lightweight aggregate concrete by replacing a part of the river sand with aeolian sand, and the influence of aeolian sand on the compressive strength of the concrete cube was studied. The results showed that the compressive strength was improved significantly when the replacement rate was between 20 and 30 %. J. C. Wu et al. [9] discussed the influence of replacing river sand with aeolian sand on the durability of concrete under the low-temperature environment. The results showed that the frost resistance of concrete increased with the replacement rate of aeolian sand, and the highest frost resistance of the concrete was found at a replacement rate of 100 %. G. T. Zhang et al. [10] analysed the effect of different replacement rates of aeolian sand on the basic mechanical properties of lithium slag polypropylene fibre concrete. The results showed that with increase in replacement rate, the compressive and splitting tensile strengths of the aeolian sand reinforced concrete both increased first and then decreased, with the optimal content at 30 %.

Compared with ordinary reinforced concrete structures, steel reinforced concrete structures have better seismic behaviours, and are becoming more widely used around the world. Many scholars have carried out a lot of research on it[11-23]. J. Y. Xue et al. [24-25] conducted the pseudo-static tests on 7 steel reinforced recycled concrete columns (Recycled concrete refers to recycled aggregate formed by crushing, screening, and washing waste concrete, partially or completely replacing natural aggregate, and then mixed with water, cement and sand in a certain proportion, setting and hardening to form the new concrete.). The results showed that the steel reinforced recycled concrete columns were applicable in practical engineering projects. The addition of recycled aggregates had little effect on the seismic behaviour of the reinforced concrete columns. J. H. Li et al. [26] carried out the low-cycle repeated loading tests on 20 steel reinforced high-strength concrete columns to study the failure morphology and seismic behaviour of the specimens, under the combined action of compression, bending, and shearing. The results showed that compared with

ordinary reinforced concrete columns, steel reinforced high-strength concrete columns showed fuller hysteresis curves with better seismic performances.

Based on the previous studies, this study combines the characteristics of steel and aeolian sand concrete structures, and proposes a built-in I-beam aeolian sand reinforced concrete column. The modified Park-Ang damage model is improved based on the analysis of the seismic behaviour, and the validity of the model is verified.

2. EXPERIMENT

2.1. SPECIMEN PRODUCTION

In this study, four steel reinforced aeolian sand concrete columns were designed and manufactured, as termed by HARC1 to HARC4. The replacement rates of aeolian sand were 10, 20, 30 and 40 %, respectively. H stands for I-steel, A represents aeolian sand, R represents reinforced concrete, and C stands for columns. The test results of four ordinary aeolian sand reinforced concrete columns (No. ARC1-ARC4) can be found in a previous study of our research group [27]. The adopted reinforcement was the same for the four specimens with the shear span ratio (the ratio of height to width of a column) of 4, the scale ratio of 1: 2, and the axial compression ratio (the ratio of the design value of the axial pressure of the column combination to the total section area of the column and the design value of the axial compressive strength of the concrete.) of 0.2. The basic parameters are listed in Table 1. The geometric dimensions and reinforcement of the specimens are shown in Figure 1. The tested elements type HARC not only meet the requirements of Code for design of composite structures, but also meet the requirements of Eurocode 4: Design of composite steel and concrete structures. The section steel and reinforcement framework were welded to the steel plate inside the column foundation to fix their positions in the aeolian sand reinforced concrete column. To ensure a close connection between the section steel and concrete, the M10×40 bolts were evenly installed along the length of the section steel, with a spacing of 100 mm. The 100 mm× 100 mm× 100 mm test cubes were poured with the specimens, and the compressive strength was measured after curing with the specimens under the same condition for 28 days.

Table 1. Basic parameters of the specimens

Specimen number	Aeolian sand replacement rate (%)	Ratio of longitudinal reinforcement (%)	Volume-stirrup ratio	Whether to contain section steel	Axial compression ratio
ARC1	10	1.20	0.006	No	0.2
ARC2	20	1.20	0.006	No	0.2

ARC3	30	1.20	0.006	No	0.2
ARC4	40	1.20	0.006	No	0.2
HARC1	10	1.20	0.006	Yes	0.2
HARC2	20	1.20	0.006	Yes	0.2
HARC3	30	1.20	0.006	Yes	0.2
HARC4	40	1.20	0.006	Yes	0.2

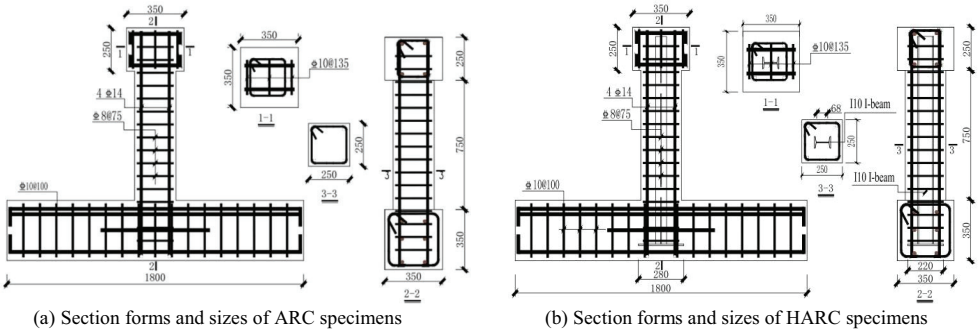


Fig. 1. The geometric dimensions and reinforcement of the specimens

2.2. MATERIAL PERFORMANCE

The raw materials used in the study included the river sand with a fineness modulus of 2.7 (The fineness modulus is an index of the size and type of natural sand.), natural pebble with a particle size from 5 to 25 mm, Jidong Cement Plant PO 42.5 cement, fly ash from Hohhot Jinshan Power Plant, naphthalene-based water-reducing agent produced by Wanshan Group, and aeolian sand in the Kubuqi Desert. The quality of these raw materials was guaranteed. The section steel adopted the type I10 real-belt ordinary hot-rolled I-beam, and the material grade was Q235. The longitudinal bars adopted the HRB400 grade rebar and the stirrup adopts HRB400 grade round steel. The section size of the column was 250 mm × 250 mm, and the properties of the steel materials are shown in Table 2. The design strength grade of the aeolian sand concrete was C40. The mixing ratio and the cubic compressive strength of the specimens can be found in Table 3.

Table 2. Mechanical indexes of the steel

Steel type	Yield strength f_y (MPa)	Ultimate strength f_u (MPa)	Elasticity modulus E_s (MPa)
I10 I-beam	345	465	1.98×10^5

Steel bar D8	450	585	2.02×10^5
Steel bar D14	479	607	2.03×10^5

Table 3. Mix ratio and strength index of the aeolian sand concrete

Aeolian sand replacement rate (%)	Amount per unit volume (kg/m^3)							Specimen cubic compressive strength (MPa)
	Cement	Sand	Aeolian sand	Aggregate	Fly ash	Water reducing agent	Water	
10	389.28	443.23	49.24	1266.36	43.62	3.27	205	36.97
20	389.28	393.99	98.48	1266.36	43.62	3.27	205	37.89
30	389.28	344.75	147.72	1266.36	43.62	3.27	205	44.1
40	389.28	295.51	196.96	1266.36	43.62	3.27	205	40.68

2.3. LOADING AND TESTING PROCEDURES

In this study, all tests were conducted in the Inner Mongolia Key Laboratory of Civil Engineering Structures and Mechanics of Inner Mongolia University of Technology. The test device is a 5000 kN loading system, as shown in Figure 2. We carried out a pre-load test before the test. The pre-load value should not be greater than 30% of the calculated cracking load. First, the vertical load was applied to the design value by the hydraulic jack. Then, the horizontal low cycle repeated load was applied to the centre of the loading beam by the horizontal actuator. The loading scheme of the load and displacement mixed control was adopted. The load control was adopted before the specimen yielded. The load increment of each grade was about 10 kN in one cycle. When the specimens yielded, the yield displacement Δ_y was increased progressively by integer multiples of the yield displacement increment, and the displacement of each stage was cycled 3 times. When the horizontal bearing capacity of the specimens dropped to about 85 % of the ultimate load or when an obvious damage occurred, the test was terminated.

The arrangement of the main measurement points of the test is as follows: linear displacement sensors were installed at the horizontal loading points (at the top of the column, half of the column height, and 10 cm above the column bottom) to determine the horizontal displacement. Three displacement meters were arranged above the ground beam and in the middle of the side to assess the fixation of the column bottom. Strain gauges (flowers) were arranged on the web of the stirrup, longitudinal rib, and section steel in the column root to measure the strain. Test data were collected by the DH3818 static strain test and analysis system.

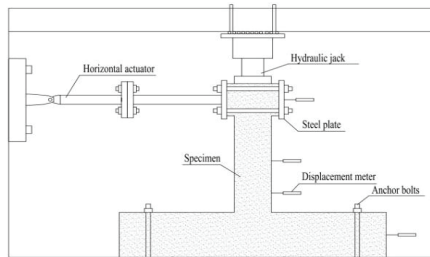


Fig. 2. Low-cycle repeated loading device

3. TEST PROCEDURE AND FAILURE CHARACTERISTICS

For specimens with large shear span ratio, their seismic behaviour is better, and both the bending failure and ductile failure can occur. In this study, all the eight specimens were showing bending failures, and the stress failure characteristics of the two groups of specimens are as follows. Figure 3 shows the bending failure of the specimens.

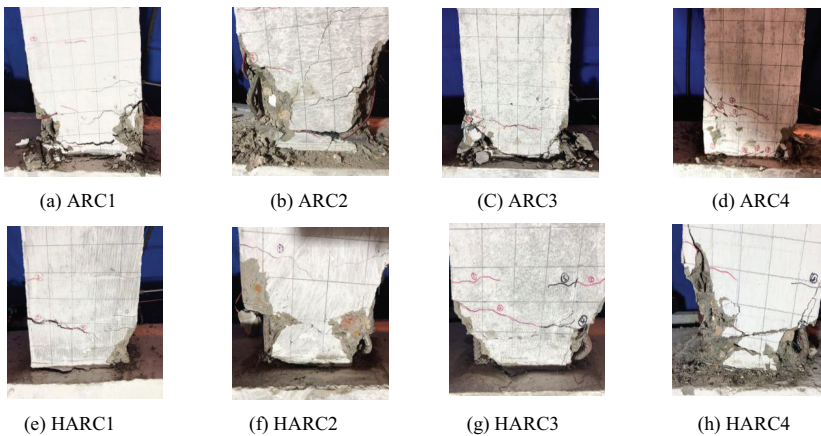


Fig. 3. Failure processes of the tested specimens

At the initial loading stage (i.e. the elastic stage) for ordinary aeolian sand reinforced concrete columns, the specimens experienced fewer load and the deformation was restored. When the horizontal load was less than the cracking load, there were a few horizontal bending cracks in the tension zone at the root of the specimens. As the loading continued, horizontal cracks extended gradually to the front and the width of the cracks continued to increase. The specimens yielded when the cracks extended to the bottom of the column. After the displacement control, a large piece of concrete was crushed at the root of the specimens and fell off with increase in the displacement. It was found that the longitudinal bars and stirrups were exposed, with the longitudinal bars also

been compressed and buckled. In addition, the horizontal bearing capacity decreased rapidly. The test was terminated when the specimens were damaged.

At the initial loading stage of loading (i.e. the elastic stage) for steel aeolian sand reinforced concrete columns, the specimens were subjected to a small load and the deformation can be generally recovered. When the horizontal load did not reach the cracking load, there were a small number of horizontal bending cracks in the tension zone of the column root. With increase in the load, the horizontal cracks extended gradually to the front. When the cracks extended to the section steel flange, some of them developed obliquely and longitudinally due to the restriction of the flange, and the development speed was relatively slow. At the same time, there were a small number of vertical cracks in the concrete outside the section steel flange of the column root. As the loading continued, the horizontal cracks increased and widened significantly to penetrate the column root with cyclic loading, and the components yielded. Then, displacement loading control was applied. With increase in the displacement under cyclic loading, the cracks increased continuously and penetrated each other on the surface of the concrete at the specimen root. With increase in the crack width, the concrete cover began to peel off and a small splitting sound was emitted inside the specimens. The horizontal load decreased when the specimens reached their maximum bearing capacities, but it decreased slowly due to the presence of internal section steel. When the displacement increased to a certain value, the longitudinal bars were bent and bulged, and a large area of the concrete was broken and fell off at the column root. The internal section steel buckled due to the loss of the protection from the concrete and the horizontal bearing capacity dropped rapidly at the same time. The test was terminated when the specimens were damaged.

4. TEST RESULTS AND ANALYSIS

4.1. HYSTERESIS CURVES

The hysteresis curve can demonstrate the comprehensive performance of seismic behaviours of the components. The measured load-displacement curves ($P-\Delta$ curves) of each specimen are shown in Figure 4. From Figure 4, the following observations can be made:

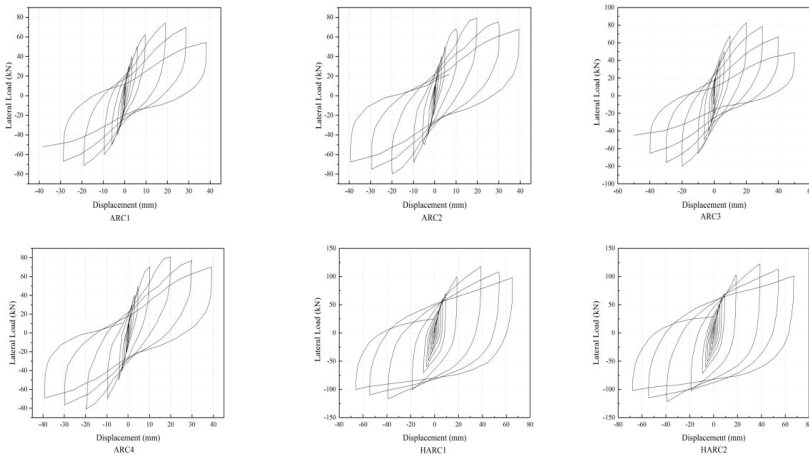
- (1) At the initial stage of loading (before cracking), the specimens were in the elastic state, and the load increased proportionally with the displacement. Most of the hysteresis curves coincided on a straight line, and the area of the hysteresis loop was relatively small. At the same time, the deformation can be generally recovered after unloading with small residual deformation.
- (2) As the loading continued, the curves inclined gradually to the displacement axis and the slope

decreased slowly with increase in the load, and the curve deformation speed increased. When the horizontal load became zero, the specimens exhibited relatively large residual deformation. At the same time, the specimens entered the elastic-plastic state.

(3) The displacement control was adopted for the specimens after yielding. As the hysteresis loop became fuller, the associated area increased. When the second-stage displacement control was $2\Delta_y$, the specimens reached the maximum horizontal load. The horizontal bearing capacity of the specimen began to decrease and the deformation became more severe. The displacement lagged during the unloading process, and the curve was almost parallel to the loading axis. When the specimen was on the verge of failure, the curve changed abruptly and the test ended.

(4) With the same replacement rate of aeolian sand, the steel aeolian sand reinforced concrete columns did not show the pinching phenomenon observed in common concrete columns, due to the existence of inner core section steel. After the ultimate loading, the horizontal bearing capacity of the specimens decreased slowly, and the hysteresis curves generally converged to those of I-steel pure steel columns. This was because the core section steel can still resist certain horizontal load after the concrete was destroyed seriously around the section steel and the steel bars yielded. In this stress mode, the section steel can be used as the second seismic defence line for the specimens to reflect the superior seismic behaviour of the section steel composite structure.

(5) It can be observed from the hysteresis curves of the HARC specimens that adding aeolian sand can lead to fuller hysteresis curves for steel reinforced concrete columns with better seismic behaviour. The replacement rate of 30 % was found to be the optimal rate, which had full hysteresis curves with a large limit displacement, followed by replacement rates of 40, 20 and 10 %.



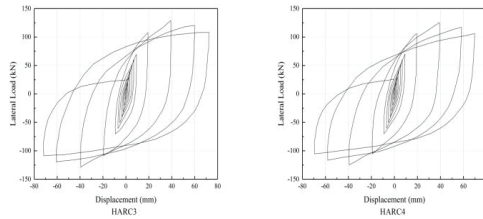


Fig. 4. Hysteresis curves of the tested specimens

4.2. SKELETON CURVES

The skeleton curve of the specimen refers to the envelope curve formed by the peak points of the first loading cycle at all levels of the load displacement curve (P - Δ curve). Figure 5 shows the skeleton curves of each specimen. The following conclusions can be drawn:

- (1) The skeleton curves of each specimen underwent the elastic stage, yield stage, strengthening stage and failure stage. The shapes of the skeleton curves of each group of the specimens were generally in similar patterns. At the initial stage of loading, the specimens were subjected to a small load in an elastic state, with the skeleton curves rising along straight lines. The initial stiffness of the HARC specimens was higher due to the presence of internal section steel, and their skeleton curves were above those of the ARC specimens.
- (2) At the same aeolian sand replacement rate, the steel reinforced concrete columns showed a greatly improved bearing capacity, greater ultimate deformation, and superior seismic behaviour, compared with the ordinary reinforced concrete columns. The descending section of the skeleton curves of HARC specimens was not as steep as those of the ARC specimens. The bearing capacity was also found to decrease slowly, which reflected good ductility.
- (3) From the skeleton curves of HARC specimens, the maximum bearing capacity of HARC specimens increased with the aeolian sand replacement rate, and the optimal replacement rate was 30 %. Therefore, within a certain range, the seismic performance of steel aeolian sand reinforced concrete structure can be improved by increasing the aeolian sand replacement rate. At the same time, the aeolian sand can be reasonably utilized to contribute to environmental protection.

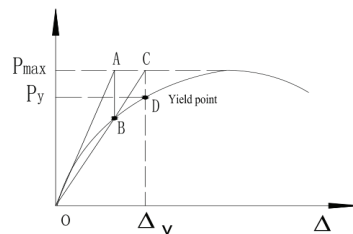
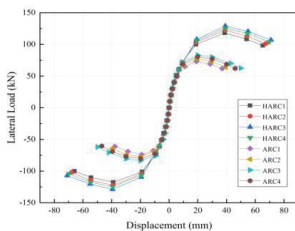


Fig. 5. Skeleton curves of the tested specimens

Fig. 6. The yield point calculated method

4.3. BEARING CAPACITY AND DUCTILITY

In this study, the ductility coefficient was used to characterize the ductility of specimens, which is given by the ratio of the ultimate deformation to the yield displacement. The ultimate deformation is the displacement when the load of the specimens drops to 85 % of the maximum bearing capacity. The yield displacement is determined by the ‘Universal Yield Bending Moment Method’, as shown in Figure 6. Over the origin point O, the elastic theory value OA line intersects the horizontal line of the maximum load at point A. Make a vertical line which goes through the point A intersects the skeleton curve at point B. Connect and extend Points O and B, intersecting the horizontal line of the maximum load at point C. Make a vertical line which goes through the point C intersects the skeleton curve at point D. The point D is the yield point. The characteristic values of load and displacement of each tested specimen under different stress state are summarized in Table 4, along with the corresponding ductility. The ultimate bearing capacity and ductility of the specimens increased first and then decreased with increase in the aeolian sand replacement rate. It was shown that we can adopt the appropriate aeolian sand replacement rate to improve the bearing capacity and ductility of steel reinforced concrete columns and to increase their seismic behaviours.

Table 4. Characteristic values of load and displacement of each test specimen and the ductility

Specimen number	Initial cracking state		Yielding state		Limit state		Failure state		Ductility coefficient μ_{Δ}
	F_{cr} /kN	Δ_{cr} /mm	F_y /kN	Δ_y /mm	F_{max} /kN	Δ_{max} /mm	F_u /kN	Δ_u /mm	
ARC1	21.6	1.51	63.79	9.25	74.83	19.1	63.56	36.73	3.97
ARC2	23.2	1.64	67.63	9.43	77.85	19.7	66.28	39.1	4.15
ARC3	24.7	1.58	69.44	9.64	83.25	19.94	70.76	42.8	4.44
ARC4	23.8	1.52	68.35	9.58	80.49	19.82	68.41	40.6	4.24
HARC1	24.1	4.29	91.16	13.68	117.92	38.72	98.2	65.2	4.77
HARC2	25.39	4.76	92.53	13.89	122.35	41.5	103.73	67.43	4.85
HARC3	30.12	4.97	94.26	14.03	128.52	43.2	109.45	71.68	5.11
HARC4	27.48	4.85	93.92	13.96	125.39	42.3	106.24	69.78	5

4.4. STIFFNESS DEGRADATION

Under the low-cycle repeated loading, the stiffness of the specimen decreased with increase in the number of loading and displacement loading cycles, due to the elastic-plastic characteristics of the specimen and the cumulative damage effect. This phenomenon is often referred as the stiffness

degradation [28]. Due to the existence of internal core steel, the initial stiffness of the specimens was relatively large. At the beginning of loading for HARC specimens, the specimens were in the elastic state before cracking, with insignificant stiffness degradation. As loading continued, the stiffness degraded to 43.4-47.2 % of the stiffness at cracking, when the specimens reached the yield stage. In the stage of displacement control, the stiffness degradation curvature increased with increase in number of loading cycles, and the curve inclined gradually to the horizontal axis with the stiffness decreased to 9.7-10.5 % of that at the time of cracking.

Figure 7 compares the stiffness degradation of all specimens at the same drift ratio. (the drift ratio is the displacement of the peak point of each cycle of the specimen divided by the height of the specimen.) Before the concrete cracking, the initial stiffness of the HARC specimens was greater than that of the ARC specimens. As loading continued, the stiffness degradation of the two groups of specimens showed obvious differences with increase in the number of cycles, but the rate of stiffness degradation accelerated significantly after entering the yield stage. The stiffness degradation curves of ARC specimens were steep and degenerated rapidly. However, the stiffness degradation curves of the HARC specimens were relatively smooth. After the concrete was crushed and peeled off and the steel bars yielded, the core steel can still resist a certain horizontal load, and the performance of the steel was relatively stable. This indicated that the stiffness degradation rate of the steel reinforced concrete specimens was smaller than that of the ordinary reinforced concrete specimens. This also showed that the steel aeolian sand reinforced concrete columns have good seismic behaviours and can be used in engineering structures with reasonable designs.

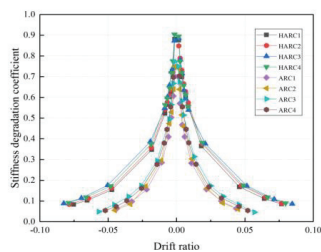


Fig. 7. Stiffness degradation coefficient curves of the specimens

4.5. ENERGY DISSIPATION

As an important means for evaluating seismic behaviours, the energy dissipation capacity of structures or members refers to the amount of energy absorbed under repeated seismic loads. In

general, the fuller and larger the hysteresis loop of the structure or component is, the stronger the energy dissipation capacity and the better the seismic behaviour. In Table 5, the equivalent viscous damping coefficient is used to measure the energy dissipation capacity of the specimens, which is calculated as follows:

$$(4.5) \quad h_e = \frac{S_{ABCD A}}{2\pi(S_{OBE} + S_{ODF})}$$

In Equation (4.5), $S_{ABCD A}$ is the area enclosed by the hysteresis curve in figure 8. $S_{OBE} + S_{ODF}$ is the sum of the area of the triangle OBE and ODF in Figure 8.

Figure 9 shows the cumulative energy consumption of each specimen, and the following can be obtained:

- (1) The equivalent viscous damping coefficient increased with increase in the displacement. In the same condition, the equivalent viscous damping coefficient of the HARC specimens was higher than that of the ARC specimens, which indicated that the HARC specimens had stronger energy dissipation capacity and better seismic behaviour. With increase in the aeolian sand replacement rate, the equivalent viscous damping coefficients of the two groups of specimen first increased and then decreased, and the 30 % replacement rate was found to be the best. It was shown that within a certain range, increasing the aeolian sand replacement rate can improve the seismic behaviour of steel aeolian sand reinforced concrete columns.
- (2) The accumulated energy consumption of the HARC specimens was significantly larger than that of the ARC specimens and adding I-beam steel can significantly improve the energy consumption capacity of aeolian sand reinforced concrete columns. The cumulative energy consumption of HARC3 was the highest, and its seismic behaviour was the best.

Table 5. Equivalent viscous damping coefficients of the specimens

Specimen number	Yield point	Peak point	Failure point
ARC1	0.031	0.111	0.21
ARC2	0.033	0.124	0.223
ARC3	0.035	0.139	0.257
ARC4	0.034	0.13	0.238
HARC1	0.202	0.291	0.311
HARC2	0.208	0.3	0.326
HARC3	0.221	0.324	0.356
HARC4	0.216	0.308	0.344

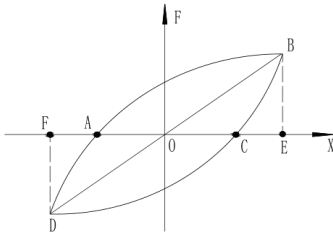


Fig. 8. Calculate the equivalent viscosity coefficient

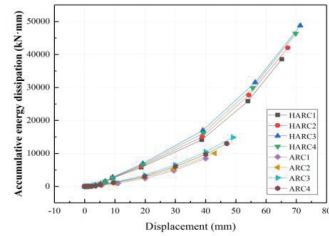


Fig. 9. Accumulative energy dissipation

5. DAMAGE ANALYSIS

5.1. SEISMIC DAMAGE MODEL BASED ON DEFORMATION

Fajfar et al. [29] believed that the damage of the structure or member was caused by the maximum elastic-plastic deformation, and they used the elastic-plastic deformation to reflect the damage, by assuming that the limit deformation under monotonous loading of the structure was equal to the limit deformation under cyclic loading. The expression can be given by:

$$(5.1) \quad D = \frac{x_m - x_y}{x_u - x_y}$$

Where x_m is the maximum elastic-plastic deformation of the component under cyclic loading; x_y is the component yield deformation under cyclic loading; and x_u is the ultimate deformation of the component under monotonic loading.

The damage index D of the HARC specimens based on deformation is shown in Figure 10. The formula of the Fajfar model is simple and easy to calculate. It can quickly calculate the damage index of specimens under different cyclic loading, and can be used as a reference for the two-parameter model.

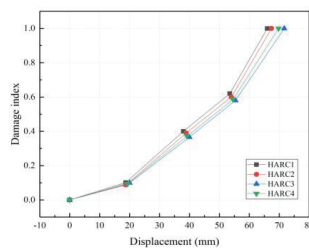


Fig. 10. Single parameter damage ratio

5.2. SEISMIC DAMAGE MODEL BASED ON DEFORMATION AND ACCUMULATIVE ENERGY DISSIPATION

The most representative two-parameter combination model is the Park-Ang model based on a large number of failure tests for reinforced concrete specimens and it can better reflect the damage law of reinforced concrete structures, despite some shortcomings. D. S. Wang et al. [30] combined the test results to analyse the relationship between the ultimate hysteresis energy dissipation of the members and the displacement ductility coefficient under cyclic loading, and they proposed an improved version form of the Park-Ang model, which is given by

$$(5.2) \quad D = (1 - \beta) \frac{\delta_m - \delta_y}{\delta_u - \delta_y} + \beta \frac{E_h}{F_y(\delta_u - \delta_y)}$$

Where δ_m is the maximum deformation of the component; δ_y is the yield deformation of the component; δ_u is the ultimate deformation of the component under monotonic loading; E_h is the actual cumulative energy consumption of the component; F_y is the bearing capacity of the component at the yield point; and β is the energy dissipation factor of the component. This model uses a non-linear combination of the maximum deformation damage term and the accumulative energy consumption damage term, which is more theoretical. The specimens are in the elastic stage without deformation damage before yielding, and the damage index is approximately 0. With increase in the displacement cycle level, the damage index gradually increases until the specimens are destroyed, and the damage index becomes 1.

Based on this model, an evaluation model for seismic damage of steel aeolian sand reinforced concrete columns was established in this study. The energy dissipation factor β is an important parameter for the modified model, by making the component damage index $D = 1$, β can be obtained as,

$$(5.3) \quad \beta = \frac{F_y(\delta_u - \delta_m)}{E_h - F_y(\delta_m - \delta_y)}$$

The ultimate deformation of specimens under monotonic loading is determined first, and formulas are given in the Research Report of the International Federation of Structural Concrete (FIB) [31].

$$(5.4) \quad \delta_u = \theta_u L$$

$$(5.5) \quad \theta_u = 0.0254 \bullet 0.3^{n_0} \left(\frac{\max(0.01, \omega')}{\max(0.01, \omega)} \bullet f_c' \right)^{0.2} \times \left(\frac{L}{d} \right)^{0.425} \times 25^{k \rho_{sx} \frac{f_{yv}}{f_c'}}$$

Where θ_u is the ultimate rotation angle of the component under monotonic loading; n_0 is the axial compression ratio of the specimen; $\omega = f_y A_s / f_c' A_g$ is the characteristic value of the longitudinal tensile reinforcement, A_g is the section area of the specimen; $\omega' = f_y' A_s' / f_c' A_g$ is the characteristic value of the longitudinal compressed reinforcement; f_c' is the compressive strength of the concrete cylinder; L/d is the shear span ratio of the specimen; ρ_{sx} is the area reinforcement ratio; f_{yv} is the strength of the stirrup; k is the effective constraint coefficient as calculated from

$$(5.6) \quad k = \frac{A_a f_a}{A_{hc} f_{hc}}$$

where A_a is the cross-sectional area of the section steel; f_a is the yield strength of the section steel; A_{hc} is the section area of the aeolian sand concrete of the specimen; f_{hc} is the compressive strength of the aeolian sand concrete cube. In this study, the following assumptions were made according to the calculation method of special-shaped steel concrete columns in the literature [32].

- (1) The conversion relationship between the cubic compressive strength f_{hc} of the aeolian sand concrete and cylindrical compressive strength f_{hc}' of the aeolian sand concrete was $f_{hc}' = 0.79 f_{hc}$;
- (2) The hysteresis curves of the specimens were approximately symmetrical in both the positive and negative directions, and the column cross-section was equivalent to the half-section steel tensile and half-section compression states, that is $\omega = \omega'$ in equation (5.5).

According to the above equation, the energy consumption factor β was obtained and substituted into Equation (5.2).

The damage index under different stress states is shown in Figure 11. For the convenience of calculating β , the non-linear fitting was performed on the energy consumption factors of the four specimens in this study. The main parameters were the aeolian sand replacement ratio, axial pressure ratio, and shear span ratio. The R^2 value of curve β is 0.77789 and the F value is 142.1248, indicating that the fitting effect of curve β is good. The expression is given by

$$(5.7) \quad \beta = 0.02164 \bullet (r)^{-0.37869} + 0.355n - 0.017\lambda$$

The following findings can be obtained from the figure:

(1) As the aeolian sand replacement increased, the damage index of the specimens gradually decreased. The damage index of the HARC3 specimen was the lowest, but the seismic behavior was the best;

(2) The modified Park-Ang damage model was improved in this study to better reflect the evolution law of seismic damage of steel aeolian sand reinforced concrete columns, and to provide an important reference for seismic damage assessment of steel aeolian sand reinforced concrete columns.

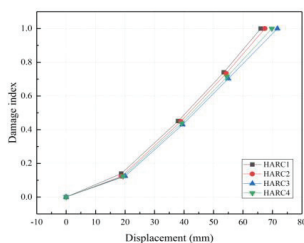


Fig. 11. Two-parameter damage ratio

6. CONCLUSIONS

This study presents an aeolian sand reinforced concrete column with I-shaped structural steel subjected to low-cycle repeated loading tests to study its seismic behavior and damage evolution process. The following conclusions can be drawn:

(1) Compared with ordinary aeolian sand reinforced concrete columns, the steel reinforced aeolian sand reinforced concrete columns have greatly improved the bearing capacity, with large ultimate deformation, more energy consumption, better ductility, and good seismic behaviours.

(2) After the concrete is severely damaged on the periphery of the section steel and the steel bars yielded, the core section steel can still resist a certain horizontal load. In this mode, the section steel can be used as the second seismic defense line of the specimens to well reflect the superior seismic behavior of the combination structure of the section steel aeolian sand concrete.

(3) The modified Park-Ang damage model has been improved in this study to better reflect the evolution law of seismic damage of steel aeolian sand reinforced concrete columns, and provide a key reference for seismic damage assessment of steel aeolian sand reinforced concrete columns.

ACKNOWLEDGMENTS : This paper was funded by the national natural science foundation of china (51868059).

REFERENCES

1. Wen-Cheng Liao, Wisena Perceka, Michael Wang, "Experimental study of cyclic behavior of high-strength reinforced concrete columns with different transverse reinforcement detailing configurations", *Engineering Structures* 153, 290–301, 2017.
2. Shenchun Xu, Chengqing Wu, Zhongxian Liu, Kunpeng Han, Yu Su, Jian Zhao, Jianchun Li, "Experimental investigation of seismic behavior of ultra-high performance steel fiber reinforced concrete columns", *Engineering Structures* 152, 129–148, 2017.
3. Shenchun Xu, Chengqing Wu, Zhongxian Liu, Ruizhe Shao, "Experimental investigation on the cyclic behaviors of ultra-highperformance steel fiber reinforced concrete filled thin-walled steel tubular columns", *Thin-Walled Structures* 140, 1–20, 2019.
4. S. W. Park, W. P. Yen, J. D. Cooper, and J. D. O'Fallon, "Seismic performance of RC bridge column under repeated ground motions", *Journal of bridge engineering*, 6: 461-467, 2001.
5. Wen-Yang Liu, Guo-Qiang Li, and Jian Jiang, "Experimental study on reinforced concrete frames with two-side connected buckling-restrained steel plate shear walls", *Advances in Structural Engineering*, DOI: 10.1177/1369433217719985, 2017.
6. Zeyang Sun, Gang Wu, Jian Zhang, Yihua Zeng, Wenchao Xiao, "Experimental study on concrete columns reinforced by hybrid steel-fiber reinforced polymer (FRP) bars under horizontal cyclic loading", *Construction and Building Materials*, <http://dx.doi.org/10.1016/j.conbuildmat.2016.10.001>.
7. Ngoc Son Vu, Bing Li, "Seismic Performance of Reinforced Concrete Columns in Corrosive Environment", *High Tech Concrete: Where Technology and Engineering Meet*, DOI: 10.1007/978-3-319-59471-2_104, 2018.
8. Dong, W., Shen, X. D., Lin, Y. J., He, J., et al. "Effect of Aeolian sand on properties of pumice lightweight aggregate concrete", *Silicate Bulletin* 34 (08): 2089-2094+2106, 2015.
9. Wu, J. C., and Shen, X. D., "Analysis of frost resistance and freeze-thaw damage mechanism of aeolian sand concrete", *Journal of Agricultural Engineering* 33 (10): 184-190, 2017.
10. Zhang, G. T., Huang, W. M., and Guo, R. "Experimental study on basic mechanical properties of polypropylene fiber concrete with desert sand lithium slag", *Science and technology and Engineering* 16 (24): 273-278, 2016.
11. Binglin Lai, J.Y. Richard Liew, "Axial-moment interaction of high strength concrete encased steel composite columns: Design recommendation", *Journal of Constructional Steel Research* 170, 106136, 2020.
12. Binglin Lai, J.Y. Richard Liew, "Design and testing of concrete encased steel composite beam-columns with C90 concrete and S690 steel section", *Engineering Structures* 220, 110995, 2020.
13. Cun Hui, Fan Zhang, Zhizeng Zhang, Xiaoli Liu, Ran Hai, John J. Myers, "Research on the Compression Behavior of Steel Reinforced Concrete Columns With Built-in Steel Tubes", *International Journal of Steel Structures*, <https://doi.org/10.1007/s13296-020-00367-9>.
14. Jianwei Zhang, Xiangyu Li, Wanlin Cao, Cheng Yu, "Cyclic behavior of steel tube-reinforced high-strength concrete composite columns with high-strength steel bars", *Engineering Structures*, 189, 565–579, 2019.
15. Binglin Lai, J.Y. Richard Liew, An Le Hoang, "Behavior of high strength concrete encased steel composite stub columns with C130 concrete and S690 steel", *Engineering Structures* 200, 109743, 2019.
16. Chenglong Wu, Sujian Yu, Jiming Liu, Genda Chen, "Development and testing of hybrid precast steel-reinforced concrete column-to-H shape steel beam connections under cyclic loading", *Engineering Structures* 211, 110460, 2020.
17. Dan Gan, Zheng Zhou, Xuhong Zhou, and Kang Hai Tan, M.ASCE, "Seismic Behavior Tests of Square Reinforced Concrete-Filled Steel Tube Columns Connected to RC Beam Joints", *Journal of Structural Engineering*, 145(3): 04018267, 2019.
18. Leo Barclay and Mervyn Kowalsky, "Seismic Performance of Circular Concrete Columns Reinforced with High-Strength Steel", *Journal of Structural Engineering*, 146(2): 04019198, 2020.
19. Cheng-Cheng Chen, Chien-Chung Chen, Thu Thuy Hoang, "Role of concrete confinement of wide-flange structural steel shape in steel reinforced concrete columns under cyclic loading", *Engineering Structures* 110, 79–87, 2016.
20. Peng Feng, Shi Cheng, and Tao Yu, "Seismic Performance of Hybrid Columns of Concrete-Filled Square Steel Tube with FRP-Confined Concrete Core", *Journal of Composites for Construction*, 22(4): 04018015, 2018.
21. Liwei Wua, Ying Tian, Youpo Sua, Haibin Chen, "Seismic performance of precast composite shear walls reinforced by concrete-filled steel tubes", *Engineering Structures* 162, 72–83, 2018.
22. Jianwei Zhang, Xiangyu Li, Wanlin Cao, Cheng Yu, "Cyclic behavior of steel tube-reinforced high-strength concrete composite columns with high-strength steel bars", *Engineering Structures* 189, 565–579, 2019.
23. Zheng Shansuo, Qin Qing, Zhang Yixin, Zhang Liang, and Yang Wei, "Research on seismic behavior and shear strength of SRHC frame columns", *Earthq Eng & Eng Vib* 16: 349-364, 2017.

24. Xue, J. Y., Lin, J. P., and Ma, H., "Experimental study on seismic behavior of recycled concrete columns", *Journal of Xi'an University of building science and Technology (NATURAL SCIENCE EDITION)* 45 (05): 615-621, 2013.
25. An He, Jian Cai, Qing-Jun Chen, Xinpei Liu, Peizhou Huang, Xu-Lin Tang, "Seismic behaviour of steel-jacket retrofitted reinforced concrete columns with recycled aggregate concrete", *Construction and Building Materials* 158, 624–639, 2018.
26. Li, J. H., Wang, X. J., Xue, J. Y., et al. "Experimental study on the mechanical properties of steel reinforced high strength concrete columns under low cyclic loading", *Journal of Civil Engineering* (07): 11-18, 2007.
27. Wang, Y. H., Chu, Q., Han, Q., et al. "Experimental study on the seismic damage behavior of aeolian sand concrete columns", *Journal of Asian Architecture and Building Engineering*, 2020.
28. Ma, H., "Study on seismic performance and design calculation method of steel reinforced recycled concrete columns", *Xi'an University of architecture and technology*, 2013.
29. FAJFAR P., "Equivalent ductility factors taking into account low-cycle fatigue", *Earthquake Engineering and Structural Dynamics* 21: 837–848, 1992.
30. Wang, D. S., Feng, Q. M., and Wang, G. X., "A modified Park-Ang seismic damage model considering low-cycle fatigue life", *China Civil Engineering Journal* 37 (11): 41-49, 2004.
31. FIB Bulletin No. 25, "Displacement-basic seismic design of reinforced concrete buildings", Lausanne: International Federation for Structural Concrete, 2003.
32. Ma, H., Guo, T. T., Xue, J. Y., et al. "Study on seismic damage model of steel reinforced recycled concrete columns based on deformation and cumulative energy consumption", *Experimental mechanics* 32 (4): 84-93, 2017.

LIST OF FIGURES AND TABLES:

Fig. 1. The geometric dimensions and reinforcement of the specimens

Fig. 2. Low-cycle repeated loading device

Fig. 3. Failure processes of the tested specimens

Fig. 4. Hysteresis curves of the tested specimens

Fig. 5. Skeleton curves of the tested specimens

Fig. 6. The yield point calculated method

Fig. 7. Stiffness degradation coefficient curves of the specimens

Fig. 8. Calculate the equivalent viscosity coefficient

Fig. 9. Accumulative energy dissipation

Fig. 10. Single parameter damage ratio

Fig. 11. Two-parameter damage ratio

Tab. 1. Basic parameters of the specimens

Tab. 2. Mechanical indexes of the steel

Tab. 3. Mix ratio and strength index of the aeolian sand concrete

Tab. 4. Characteristic values of load and displacement of each test specimen and the ductility

Tab. 5. Equivalent viscous damping coefficients of the specimens